[51]L. D. Landau and E. M. Lifshitz, *Quantum Mechanics* (Pergamon, London, 1958), Appendix d.
[52]B. E. Springett, J. Jortner, and M. H. Cohen, J. Chem. Phys. 48, 2720 (1968).
[53]T. Miyakawa and D. L. Dexter, Phys. Rev. 184, 166 (1969).
[54]K. R. Atkins, Can. J. Phys. 31, 1165 (1953).
[55]L. P. Pitaevskii, Zh. Eksperim. i Teor. Fiz. 31, 536 (1956)[Soviet Phys. JETP 4, 439 (1956)].
[56]J. Lekner, Phys. Rev. 158, 130 (1967).
[57]See e.g., Y. L. Luke, in *Handbook of Mathematical Functions*, edited by M. Abramowitz and I. A. Stegun (Dover, New York, 1965).
[58]M. W. Cole, Phys. Rev. A1, 1838 (1970).
[59]A. Widom, Phys. Rev. A1, 216 (1970).
[60]R. E. Prange [Phys. Rev. 187, 804 (1969)] has considered this interaction in a similar context.
[61]R. F. Greene and R. W. O'Donnell, Phys. Rev. 147, 599 (1966).
[62]C. B. Duke, Phys. Rev. 168, 816 (1968).
[63]See, e.g., G. Wendt, in *Handbuch der Physik*, XVI, edited by S. Flugge (Springer-Verlag, Berlin, 1958), p. 28.

PHYSICAL REVIEW B VOLUME 2, NUMBER 10 15 NOVEMBER 1970

Isotope Splitting of the *F*-Center In-Gap Mode in KI and KBr

D. Bäuerle*†‡
Laboratory of Atomic and Solid State Physics, Cornell University, Ithaca, New York 14850
and
R. Hübner§
Institut für theoretische Physik, der Universität Stuttgart, Germany
(Received 30 March 1970)

High-resolution measurements at the *F*-center in-gap mode in KI and KBr have revealed a threefold structure in the absorption spectrum with lines at 82.62 ± 0.02, 81.98 ± 0.02, 81.19 ± 0.05 cm^{-1} and at 99.60 ± 0.03, 99.07 ± 0.04, 98.50 ± 0.05 cm^{-1}, respectively. This structure is interpreted as due to the presence of two stable isotopes, K^{39} and K^{41}, in the crystal. In a three-dimensional-model calculation which uses as parameters changes in the force constants between the defect and the first nearest neighbors ($A01$) and changes in the force constant between the first and fourth nearest neighbors ($A14$), we found that the in-gap mode frequencies are extremely sensitive to the value of the latter. The position and splitting in the absorption lines can be explained in the calculation by using $A01 = -0.50$, $A14 = -0.060$ for KI and $A01 = -0.50$, $A14 = +0.002$ for KBr. Stress experiments on the strongest lines in KI are in agreement with our model. Extending the calculation to Cl^- and Br^- centers in KI, it is shown that the measured isotope splitting for Cl^{35}, Cl^{37} and Br^{79}, Br^{81} centers can be explained by taking into account not only changes in $A01$ but also changes in $A14$.

I. INTRODUCTION

The far-infrared absorption spectra associated with very light substitutional defects in alkali halides like H^-, D^- ions (U centers) and F, F' centers were recently reported.[1–4] These vacancy-type centers give rise to resonance absorption in the upper acoustic band for H_s^-, D_s^-, and F' centers and to gap-mode absorption in the region between the optic and acoustic phonon branches for the F center, respectively. The different absorption frequencies of these defects are mainly an effect of local force-constant changes. The amount by which the perturbed force constants differ from the unperturbed value can be obtained by fitting the experimental results to model calculations in three dimensions. Calculations of the infrared-active modes in perturbed lattices on the basis of "realistic models" for the lattice dynamics are given, e.g., by Klein,[5] Page and Strauch,[6] Benedek and Nardelli,[7] and some others. Recently, Benedek and Mulazzi[8] calculated the F-center gap-mode absorption based on one of Hardy's deformation dipole models.

The measurements and calculations reported in this paper should provide further clarification of the dependence of the optical response of perturbed lattice vibrations on mass and force-constant changes. As a "model case," we have chosen the F center for the following reasons: (a) Some lattice dynamical properties of the F center are already known. They could be studied indirectly through the electronic transition because of the electron-phonon interaction.[8–10] (b) The vibrational absorption associated with F centers in KBr and KI is in the phonon gap. Therefore, the corresponding absorption lines are sharp, and small perturbations of the surrounding lattice can be measured.

After a short description of the experimental apparatus (Sec. II), we present in Sec. III the experimental results. High-resolution measurements at the F-center in-gap mode in KI near 83 cm^{-1} have revealed a threefold structure of the absorption shape. Quite similar lines occur in KBr (Sec. III A). Stress experiments at the strongest lines in KI, those at 82.62 and 81.98 cm^{-1}, are reported in Sec. III B.

In Sec. IV a short discussion of the theoretical background and the assumptions entering the numerical calculations is given. In these analyses we make use of the breathing shell model for alkali halides as described by Schröder.[11] As a test of the model and the macroscopic parameters used in the calculation, we compare the neutron scattering data ($T = 95\,^{\circ}$K) for the dispersion curves of KI as given by Dolling *et al.*[12] (see Appendix).

The numerical results of our calculation for the F center are reported and discussed in Sec. V. The observation of three absorption lines in the gap region of KI and KBr with F centers is interpreted by the presence of two stable potassium isotopes K^{39} and K^{41} in the crystal. The single lines can be attributed to defect-center configurations, in which zero, one, or two of the six nearest neighbors of the F center are replaced by the heavier isotope. From this assumption an estimate of the force-constant changes around the center can be made (Sec. V A).

A qualitative discussion of the stress experiments is in agreement with the above interpretation of the triple absorption structure. Furthermore, an estimate of the anharmonic coupling coefficients is given (Sec. V B).

In Sec. VI, we compare the force-constant changes around the F center obtained in Sec. V A with the corresponding values reported in Ref. 8. Finally, as a test of the logic of Sec. IV, we apply our model calculation to Cl^- and Br^- centers in KI, and compare the results with those obtained in Ref. 13.

II. EXPERIMENTAL

A. Spectrometer

The measurements have been carried out partially with a commercial Fourier spectrometer (RIIC) using a Golay cell and partially with a homemade system[14] which uses a He^4-cooled bolometer detector.[13] The latter spectrometer consists of an aperiodic 2-in. Michelson interferometer, which was built in a nonrectangular fashion as described by Genzel.[15] The optical part of the RIIC instrument (FS 720), is an aperiodic 2-in. Michelson interferometer also, but with the primary rectangular arrangement. The resolution with an RIIC instrument was originally determined by the storage capacity of the Fourier-transform computer unit FTC 100. It was increased by punching the digitized detector signal, the interferogram $I(\gamma)$ of the transmitted spectral distribution $S(\nu)$,

$$I(\gamma) = \int_0^\infty S(\nu)\cos 2\pi\nu\gamma\, d\nu + \tfrac{1}{2} I(0) \qquad (2.1)$$

in the region $0 \approx \gamma \leq L$, on tape. Because the FS 720 interferometer cannot be symmetrized to the position $\gamma = 0$, it was necessary to determine later the value $I(0)$ and the phase error ϵ from the punched interferogram. A parabolic fit for determining the white-light position led to satisfactory spectra; for that purpose $I(\gamma)$ was punched in the whole γ region with a sampling $h' = \frac{1}{2}h$ or $h' = \frac{1}{3}h$ ($h = 1/2\nu_M$, ν_M = cutoff frequency, which was produced in the following measurements by 2-mm wedged crystalline quartz and the intrinsic absorption of the crystal itself). Then in $I(\gamma)$ the largest and second-largest value served for a parabolic fit. The ordinate of the parabola was used as the corrected position $I(0)$, the transformation was then done according to

$$S(\nu_M) = 2\sum_{n=1}^{N} A(nh+\epsilon)\left[I(nh+\epsilon) - \tfrac{1}{2}I(0)\right] \times \cos[2\pi\nu(nh+\epsilon)]. \qquad (2.2)$$

$N+1$ equals the total number of values which were used for the transformation. $I(nh)$ is the intensity at $\gamma = nh$. Usually a triangular apodization $A(nh) = (1 - n/N)$ was used. Because in the following measurements we were only interested in a very small frequency region, in all cases expression (2.2) was calculated by the "direct sum" algorithm. In this manner the transformation (2.2) for a frequency range of 5 cm^{-1} using 1800 points, required about 90 sec on an IBM 360/60 computer.

With the RIIC instrument, for a resolution of $1/Nh \approx 0.15$ cm^{-1} in the apodized spectrum a signal to noise $S/N \approx 6$ was obtained. This resolution was verified by the water-vapor doublet at 55 cm^{-1} (0.29-cm^{-1} separation) and at the Cl^- in-gap mode in KI near 77 cm^{-1} (isotope splitting 0.31 cm^{-1} with Cl^{35} and Cl^{37}, respectively).

The homemade instrument could be symmetrized to the position $\gamma = 0$. The bolometer signal at points $\gamma = nh$ was digitized and punched on cards. The transformation was done according to (2.2) with $\epsilon = 0$. With a resolution of 0.1 cm^{-1} we obtained a $S/N \approx 50$.

In both cases, with the RIIC and the homemade instrument, the agreement in the main absorption frequencies of the F-center doublet was better than ± 0.05 cm^{-1}.

B. Crystals, Center Production

KBr and KI single crystals were grown by the Kyroupolos method in an argon atmosphere. F centers were usually produced by X irradiation of crystals containing U centers; however, quenched additively colored crystals as well as "pure" x-irradiated crystals were also used. The main features of the spectra were in all cases the same.

The samples used in the stress experiments were doped with 0.1-mole% CaI_2.

III. EXPERIMENTAL RESULTS

A. High-Resolution Spectra

Figure 1 shows the in-gap-mode absorption of F centers in KI with an instrumental resolution of 0.1 cm^{-1}. The spectrum was obtained by comparing the transmission of "doped" and "undoped" samples.

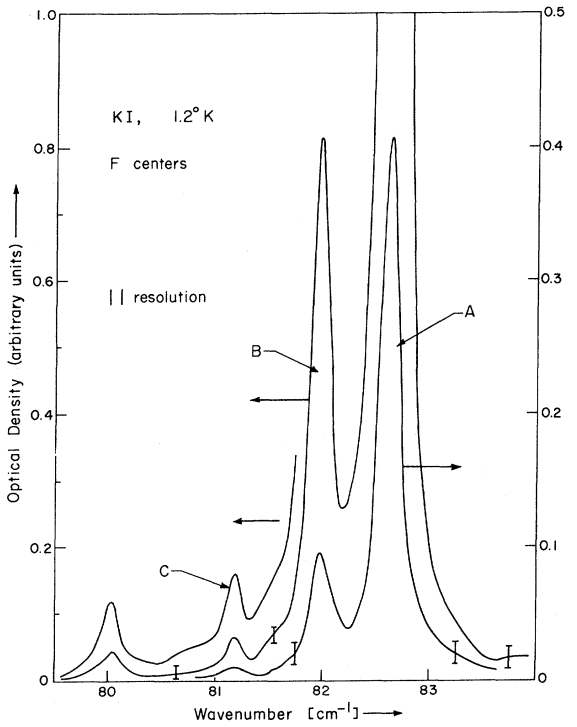

FIG. 1. F-center in-gap mode in KI with a resolution of 0.1 cm^{-1} (apodized spectrum). The positions of the lines are: $A = 82.62 \pm 0.02$ cm^{-1}; $B = 81.98 \pm 0.02$ cm^{-1}; $C = 81.19 \pm 0.05$ cm^{-1}.

The most remarkable feature is the strong doublet with peak frequencies at 82.62 ± 0.02 and 81.98 ± 0.02 cm^{-1}. The relative intensities of these lines are constant and independent of the method of F-center production. No concentration-dependent frequency shift in these main lines was observed on changing the F-center concentration between 10^{17} and 3×10^{18} cm^{-3}. Furthermore, in additively colored crystals when converting F centers to M centers (at 300 °K by irradiation of the crystal with F-center light) both components of the doublet decrease together. No further sharp absorption occurs in the gap.

In order to clarify the absorption shape beyond the strong doublet, very thick samples (up to 10 mm) containing 3×10^{18} cm^{-3} F centers were used (curve c). For this purpose, samples containing U centers were sliced, x irradiated and put together. For avoiding interferences of the infrared beam, the cutting planes were chosen parallel to the propagation direction of the light. In all crystals, two more lines were observed with peaks at 81.19 ± 0.04 and 80.05 ± 0.04 cm^{-1}. These lines also seem to be proportional to the F-center concentration. However, the 80.05-cm^{-1} line is probably due to a perturbation of F centers by Na^+ ions. This was checked in preliminary experiments with F_A (Na) centers.

The ratio of the integral absorptions, $I = \int \alpha(\nu)\, d\nu$ of the three remaining lines, henceforth noted as A, B, and C, is experimentally

$$I(A = 82.62) : I(B = 81.98) : I(C = 81.19)$$
$$= 193 : (28 \pm 10\%) : (1 \pm 25\%). \qquad (3.1)$$

The temperature dependence of the line intensities has been measured from 1.2 to 18 °K with an instrumental resolution of 0.3 cm^{-1}. Within the accuracy of our measurements, the intensities do not change appreciably with increasing temperature. Only the flat background absorption becomes stronger because of the rise of "difference processes" in the phonon spectrum. This temperature behavior of the F-center–induced in-gap mode is in agreement with analogous temperature measurements at the Cl^- in-gap mode in KI as observed by Nolt *et al.*[13]

In KBr, a similar absorption shape for the F in-gap–mode absorption is shown in Fig. 2. The peak frequencies are $A = 99.60 \pm 0.03$, $B = 99.07 \pm 0.03$, and $C = 98.50 \pm 0.05$ cm^{-1}. In this case, for the relative integral absorption strength we obtained

$$I(A = 99.60) : I(B = 99.07) : I(C = 98.50)$$
$$= 130 : (21 \pm 20\%) : (1 \pm 50\%). \qquad (3.2)$$

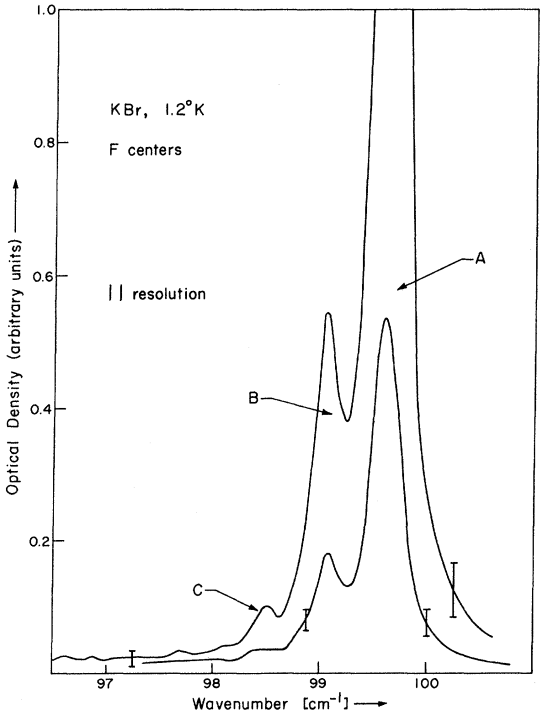

FIG. 2. The same as in Fig. 1, but for KBr. The positions of the lines are $A = 99.60 \pm 0.03$ cm^{-1}; $B = 99.07 \pm 0.04$ cm^{-1}; $C = 98.50 \pm 0.05$ cm^{-1}.

This is, within the error of our analysis, the same as for the case of KI. As outlined in Sec. V A, the frequencies and relative intensities of the single peaks of the F in-gap-mode absorption in KI and KBr can be explained by the presence of two isotopes in the crystal, K^{39} and K^{41}, which are in a natural ratio $K^{39}:K^{41}=93:7$. This interpretation could be tested experimentally by using isotopically pure crystal materials, but the cost of such an experiment would be prohibitive.

B. Uniaxial Stress Experiments

Stress experiments have been carried out at the strongest lines of the F-center in-gap mode in KI, those at $A=82.62$ cm^{-1} and $B=81.98$ cm^{-1}. The relative frequency shift in the lines, $\Delta\nu=\nu-\nu_0$, as a function of pressure is shown in Fig. 3 for $E\parallel P\parallel[100]$ and $E\parallel[001]$, $P\parallel[100]$. E is the electric vector of the incident light and P is the uniaxial stress. As can be seen in Fig. 3, each line of the doublet splits into two components which shift linearly with applied stress but by different amounts. We obtained the following:

(a) for the $A=82.62$-cm^{-1} line,

$$E\parallel P:\ \Delta\nu_1(A)/P=(0.11\pm0.03)\times10^{-2}\ \text{cm}^{-1}/\text{kg}\ ,$$

$$E\perp P:\ \Delta\nu_2(A)/P=(0\pm0.04)\times10^{-2}\ \text{cm}^{-1}/\text{kg}\ ;$$

(b) for the $B=81.98$-cm^{-1} line,

$$E\parallel P:\ \Delta\nu_1(B)/P=(0.15\pm0.02)\times10^{-2}\ \text{cm}^{-1}/\text{kg}\ ,$$

$$E\perp P:\ \Delta\nu_2(B)/P=(-0.01\pm0.03)\times10^{-2}\ \text{cm}^{-1}/\text{kg}\ .$$

Within the accuracy of our measurements in these experiments no change in the band shape as well as the integral absorption ($\pm30\%$) was observed.

IV. THEORETICAL MODELS

A formulation of the theory of infrared absorption of crystal lattices with point defects is reviewed by several authors (see, e.g., Klein,[5] Benedek and Nardelli[7]).

The linear absorption coefficient is given by

$$\alpha_{xy}(\omega)=4\pi(\omega/c)\,\text{Im}\,\chi_{xy}(\omega)\ . \tag{4.1}$$

In the notation used in Refs. 5 and 7, the susceptibility is written as

$$\chi=(NZ^2/\mu v_0)\times\lim_{\epsilon\to+0}[\tilde{\varphi}_{TO}|(G_0^{-1}+pG_0^{-1}TG_0)^{-1}|\tilde{\varphi}_{TO}]$$

$$=(NZ^2/\mu v_0)\times\lim_{\epsilon\to+0}\{[\omega_{TO}^2-(\omega+i\epsilon)]^2+p(\tilde{\varphi}_{TO}|T|\tilde{\varphi}_{TO})\}^{-1}\ , \tag{4.2}$$

with $T=V(I+G_0V)^{-1}$. N is the total number of cells, v_0 is the volume of a cell, Z is the ionic charge, and μ is the reduced mass:

$$\mu=m_+m_-/(m_++m_-)\ . \tag{4.3}$$

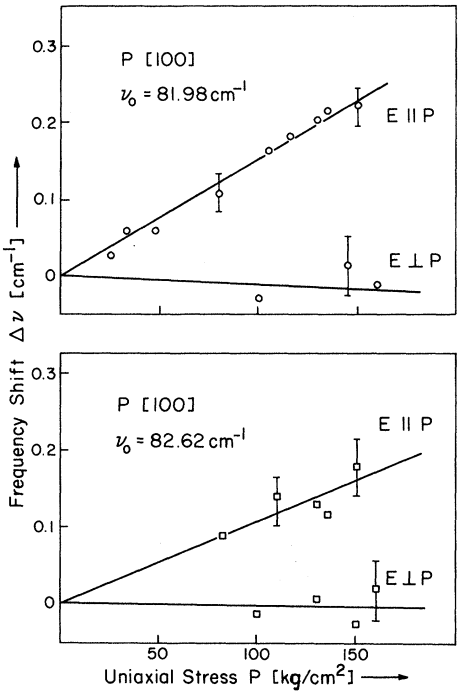

FIG. 3. Frequency shift $\Delta\nu=\nu-\nu_0$ of the lines A ($\nu_0=82.62$ cm^{-1}) and B ($\nu_0=81.98$ cm^{-1}) of the F-center in-gap mode in KI (5 °K) with uniaxial stress.

G_0 is the Green's function matrix, and V the defect matrix, and p is the probability of finding one defect center in one cell. In KI with $v_0=2a_0^3=84.944\times10^{-24}$ cm^3, $p=0.001$ corresponds to a concentration of 1.18×10^{19} centers/cm^3.

To simplify the calculation of the T-matrix elements we introduce special symmetry vectors (shell vectors), which are described in more detail in Refs. 9 and 16. These shell vectors constitute a complete set of basis functions and are most suitable for describing the lattice vibrations around a defect with a finite range of perturbation. In a lattice with point-symmetry group H the lattice ions may be assumed to be arranged on "shells" around the defect. A "shell" is defined by all lattice points which transform into one another under all symmetry operations of H.[17] Shell vectors σ_ν are those basis vectors to irreducible representations of H, the amplitudes of which are nonzero only on a single shell.

To describe the shell vectors completely, four indices are necessary:

$$\sigma_\nu=\sigma(\Gamma,\ j;\ s,\ r)\ , \tag{4.4}$$

where s is the shell number, starting with $s=0$ for the defect itself, Γ gives the irreducible representation of H, r the index of multiplicity of Γ in the shell s, and j is the index of degeneracy, which

counts the different basis functions within one representation Γ.

We now obtain the following projections:

$$s_\nu = s(\Gamma, j; s, r) \equiv (\tilde{\varphi}_{\mathrm{TO}} | \sigma(\Gamma, j; s, r)) \ ;$$
$$\hat{T} = (\sigma | T | \sigma') = (\sigma | V(1 + G_0 V)^{-1} | \sigma')$$
$$= \sum_{\sigma''} (\sigma | V | \sigma'')(\sigma'' | R | \sigma') \equiv \hat{V} \cdot \hat{R}. \qquad (4.5)$$

Next we calculate the scalar product $\langle s | \hat{T} | s \rangle$, where the multiplication runs over all nonzero projections $(\tilde{\varphi}_{\mathrm{TO}} | \sigma)$. With the abbreviation[7]

$$\langle s | \hat{T} | s \rangle = (N_1 + iN_2)/(D_1 + iD_2) \ , \qquad (4.6)$$

the absorption outside the unperturbed phonon bands reads $\mathrm{Im}(\sigma | G(\epsilon \to 0) | \sigma') = 0$:

$$\alpha(\omega_L) = \frac{4\pi}{c} \omega_L \lim_{\epsilon \to +0} \mathrm{Im}\chi(\omega_L)$$
$$= \frac{4\pi}{c} \omega_L \frac{N Z^2}{\mu v_0} \lim_{\epsilon \to +0} \frac{\epsilon}{(\omega_{\mathrm{TO}}^2 - \omega^2 + p N_1/D_1)^2 + \epsilon^2}$$
$$= \frac{4\pi}{c} \omega_L \frac{N Z^2}{\mu v_0} \pi p \frac{N_1(\omega_L)}{(\omega_{\mathrm{TO}}^2 - \omega^2)}$$
$$\times \delta[(\omega_{\mathrm{TO}}^2 - \omega^2) D_1(\omega_L) + p N_1(\omega_L)] \ . \qquad (4.7)$$

In the following we will discuss Eqs. (4.5) and (4.6) for some models of special centers (F, Cl^-, Br^- in KI). The changes of ion masses, force constants (as far as the short-range parts are concerned), and the related symmetries of the mass systems will be considered. All perturbations in the effective charges of the ions will be neglected,[18] which means that in the perturbed lattice only those infrared-active modes which can be deduced from the $\Gamma_4^-(T_{1u})$ modes of the unperturbed lattice will contribute to the absorption coefficient. In Eq. (4.5), $s_\nu \neq 0$ is valid only if $\sigma_\nu = \sigma(\Gamma_4^-, j; s, r)$. Hence we obtain

$$\langle s | = \langle s(\Gamma_4^-), \ s(\Gamma) | = \langle s(\Gamma_4^-), \ 0 | . \qquad (4.8)$$

In the same way we split the projections of the perturbation matrix V and the Green's function G:

$$\hat{V} = \begin{bmatrix} \hat{V}(\Gamma_4^-) & \hat{V}(\Gamma_4^-, \Gamma) \\ \hat{V}(\Gamma, \Gamma_4^-) & \hat{V}(\Gamma) \end{bmatrix} \ , \qquad (4.9)$$

$$\hat{R} = \begin{bmatrix} 1 + \hat{G}(\Gamma_4^-)\, \hat{V}(\Gamma_4^-) & \hat{G}(\Gamma_4^-, \Gamma)\, \hat{V}(\Gamma) \\ \hat{G}(\Gamma, \Gamma_4^-)\, V(\Gamma_4^-) & 1 + \hat{G}(\Gamma)\, V(\Gamma) \end{bmatrix}^{-1} . \qquad (4.10)$$

G_0 is a fully cubic matrix, so that all mixing between different representations Γ vanish [$G(\Gamma_4^-, \Gamma) = 0$]:

$$\hat{R} = \begin{bmatrix} (1 + \hat{G}(\Gamma_4^-)\, \hat{V}(\Gamma_4^-))^{-1} & \\ & (1 + \hat{G}(\Gamma)\, \hat{V}(\Gamma))^{-1} \end{bmatrix} , \qquad (4.11)$$

and we obtain

$$\langle s | \hat{T} | s \rangle = \langle s(\Gamma_4^-) | \hat{V}(\Gamma_4^-) [1 + \hat{G}(\Gamma_4^-) \hat{V}(\Gamma_4^-)]^{-1} | s(\Gamma_4^-) \rangle \ . \qquad (4.12)$$

To find the only unknown in Eq. (4.12) we have to discuss the projected perturbation matrix $\hat{V}$, and the vector $\langle s(\Gamma_4^-)|$ for special models.

We define A and B to be the radial and tangential force constants of the ideal lattice, respectively. They may contain central as well as noncentral parts (see, e.g., Ref. 19). $A_{ss'}$ and $B_{ss'}$ ($\Delta A_{ss'} = A_{ss'} - A$, $\Delta B_{ss'} = B_{ss'} - B$) are the constants of the perturbed lattice connecting shells s and s'.

In the following cases we neglect changes in the tangential force constant B, since $B \lesssim \frac{1}{10} A$.

A. Case 1

An anion center with mass changes and force-constant changes to ($1nn$) and ($4nn$):

$$m_-' \gtrless m_- ; \quad \epsilon_- = 1 - m_-'/m_- ; \quad \Delta A_{01} \neq 0 ; \quad \Delta A_{14} \neq 0 ;$$

but in an environment of O_h symmetry.

If there exists a $\Gamma_4^-(T_{1u})$ representation in one shell more than once, the shell vectors may be chosen in such a way that they project either on radial or tangential force-constant changes only. With $\Delta B_{ss'} = 0$ we have to deal with the radial representations only. For $s = 0$, 1, 4 we obtain three representations and the symmetry vectors are $\sigma(\Gamma_4^-, j; 0)$, $\sigma(\Gamma_4^-, j; 1, 1)$, $\sigma(\Gamma_4^-, j; 4, 1)$, with $j = 1$, 2, 3:

$$\langle S |_x = \langle s(\Gamma_4^-, 1; 0); \ s(\Gamma_4^-, 1; 1, 1); \ s(\Gamma_4^-, 1; 4, 1); \ 0 | = N^{-1/2} (m_+ + m_-)^{-1/2} \langle -m_+^{1/2}; \ (2m_-)^{1/2}; \ -(2m_+)^{1/2}; \ 0 | \qquad (4.13)$$

(we give only the x components of the polarization);

$$\hat{V} = \begin{bmatrix} \hat{V}_x & & \\ & \hat{V}_y & \\ & & \hat{V}_z \end{bmatrix} ; \quad \hat{V}_\alpha \text{ symmetric};$$

$$\hat{V}_\alpha^{(1)} = \begin{bmatrix} \epsilon_- \omega^2 + \Delta A_{01}/m_- & -\sqrt{2}\, \Delta A_{01}/(m_+ m_-)^{1/2} & 0 \\ \cdots & (\Delta A_{01} + \Delta A_{14})/m_+ & -\Delta A_{14}/(m_+ m_-)^{1/2} \\ \cdots & \cdots & \Delta A_{14}/m_- \end{bmatrix} . \qquad (4.14)$$

All gap modes in this case are threefold degenerate, but their total number cannot be predicted without a numerical investigation. Modes of that character will be discussed in Secs. V and VI for the F center and for Cl^- and Br^- centers in KI.

B. Case 2

Same as case 1, but with additional mass changes in the first shell. The force-constant changes still have O_h symmetry; the perturbation masses may reduce the symmetry to C_{4v}, D_{4h}, or C_{2v}, depending on whether there are one or two new masses on $(1nn)$ sites.

For $m'_+ \gtrless m_+$ and $\epsilon_+ = 1 - m'_+/m_+$, the s vector of the first example is not altered.

Case 2(a)

For one mass m'_+ at $(1nn)$ site, C_{4v}:

The V projection reads

$$\hat{V}_x^{(2)} = \hat{V}_y^{(2)} = \hat{V}_x^{(1)};\ \hat{V}_z^{(2)} = \hat{V}_z^{(1)} + \begin{bmatrix} 0 & & \\ & \frac{1}{2}\epsilon_+\omega^2 & \\ & & 0 \end{bmatrix}. \quad (4.15)$$

We get two types of modes: the unperturbed modes of the first model (twofold degenerate) and one nondegenerate new mode. That case will be discussed later for the F center in KI considering the natural mixture of K^{39} and K^{41} isotopes in the crystal.

If there are two K^{41} isotopes within the first shell, we have to distinguish two cases.

Case 2(b)

For two masses m'_+ at $(1nn)$ sites [e.g., one at (001), the other at (010)], C_{2v}:

We find

$$\hat{V}_x^{(2)} = \hat{V}_x^{(1)};\ \hat{V}_y^{(2)} = \hat{V}_z^{(2)} = \hat{V}_z^{(1)} + \begin{bmatrix} 0 & & \\ & \frac{1}{2}\epsilon_+\omega^2 & \\ & & 0 \end{bmatrix}. \quad (4.16)$$

This result yields no new structure in comparison to case 2(a). Only the degeneracies are interchanged.

Case 2(c)

For two masses m'_+ at $(1nn)$ on opposite lattice sites D_{4h}. We obtain

$$\hat{V}_x^{(2)} = \hat{V}_y^{(2)} - \hat{V}_x^{(1)};\ \hat{V}_z^{(2)} = \hat{V}_z^{(1)} + \begin{bmatrix} 0 & & \\ & \epsilon_+\omega^2 & \\ & & 0 \end{bmatrix}. \quad (4.17)$$

We find two types of modes. The degeneracy is the same as in case 2(a), but the splitting is larger.

No further gap modes can occur in connection with the heavier-mass isotope K^{41}. All $\Gamma_4^-(T_{1u})$ modes which strain the force constants between $1nn$ and $2nn$ correspond to the case of diatomic linear chain with $m_+ < m_-$ and $\epsilon_+ < 0$, where no gap modes exist (see, e.g., Ref. 20).

V. DISCUSSION

Before comparing in detail the experimental results of Sec. III with the model calculation of Sec. IV, we make some general remarks which follow from the numerical investigations.

As may be seen from Figs. 4, 5, 7, and 8, the positions of the gap modes depend strongly on $A14$, the force-constant change between $1nn$ and $4nn$, even in the case of Cl^- and Br^- centers in KI. For any fixed value of $A01$ the peaks may be shifted over the total gap region by a variation of $A14$ within reasonable limits ($-0.3 < A14 < 0.3$; $A14 = A_{14}/A - 1$; $A_{01} = A_{01}/A - 1$). This indicates that a realistic model for the description of infrared absorption of defect centers should not be restricted too much in local space. A larger region around the center will be changed (at least up to $4nn$) by the relaxation of the surrounding lattice. This statement seems to be true for the "soft" F center as well as for such "simple" centers as Cl^- and Br^- ions in KI.

Moreover, because of the similar behavior of different centers, we suggest that the most important contribution to $A14$ is from the relaxation of $1nn$ and not due to the special electronic structure

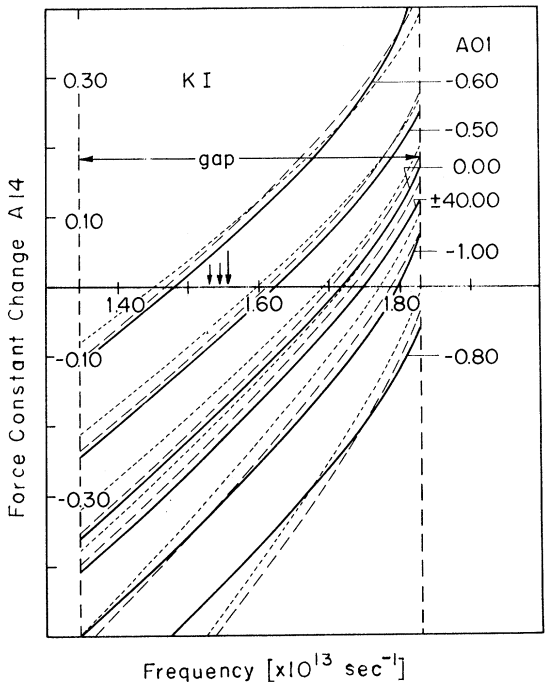

FIG. 4. Dependence of the line position and splitting of the F-center gap mode absorption in KI as a function of force-constant changes $A01$ and $A14$: solid line F centers in the $b(0)$ configuration; dashed line F centers in the $b(1)$ configuration; dotted line F centers in the $b(2)$ configuration. The calculation was done for $T = 0$ °K. The arrows show the experimental positions of lines.

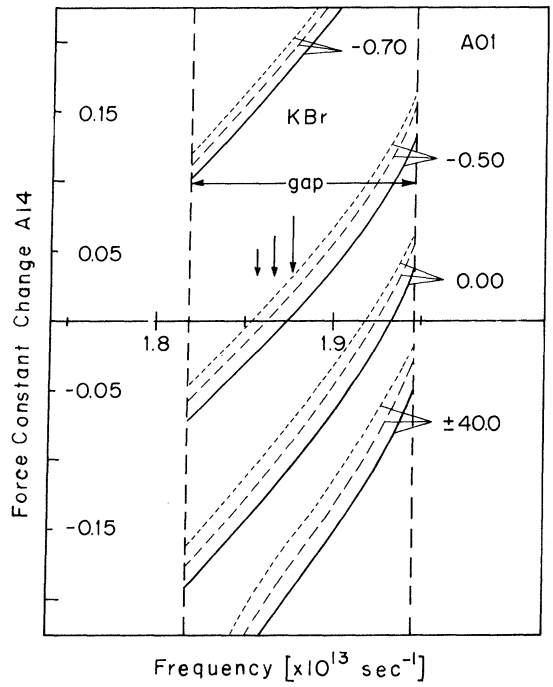

FIG. 5. Same as for Fig. 4, but for KBr.

of the defect (e.g., the widely spread electronic wave function of the F center). Changes in the charge distribution of the outer electron of the defect are shared among all neighbors, therefore contributing little to $A14$.

A. Positions and Relative Intensities of F-Center Lines

The frequencies of the single lines of the F-center-induced gap-mode absorption in KI and KBr of Sec. III A are given by the model calculations outlined in Sec. IV B.

For the case of KI we show in Fig. 4 the position of the three lines as a function of the parameters $A01$ and $A14$. A fit of the observed frequency $A = 82.62\ \text{cm}^{-1}$ [$\omega_A = (1.556 \pm 0.001) \times 10^{13}\ \text{sec}^{-1}$] for the main line of Fig. 1 restricts the possible $A01$, $A14$ force-constant pairs to a range which is given to a good approximation by the empirical equations

$$A14 = -\frac{0.21\,A01 + 0.118}{A01 + 0.715} \quad \text{for } A01 > -0.715,$$

$$A14 = -\frac{0.21\,A01 + 0.130}{A01 + 0.715} \quad \text{for } A01 < -0.715.$$

An additional fit of the measured splitting $\Delta_{AB} = 0.64\ \text{cm}^{-1}$ in the doublet gives a further restriction of $A01$ to the interval $-0.60 < A01 < 0$ (see Table I), and thereby restricts $A14$ to negative values as well. The negative value for $A14$ is interpreted as an increase of the distance between $1nn$ and $4nn$, caused by a decrease of the distance between the F center and $1nn$. The line at $C = 81.19 \pm 0.04\ \text{cm}^{-1}$ [$\omega_C = (1.529 \pm 0.001) \times 10^{13}\ \text{sec}^{-1}$] is best reproduced by setting $A01 = -0.50$ and $A14 = -0.060$.

For the case of KBr, the analogous calculations are shown in Fig. 5 and Table II, respectively. In this case, the calculated splitting Δ_{AB} and Δ_{AC} are nearly constant over the whole range of $A01$, $A14$ pairs, but somewhat smaller than for KI. This smaller splitting is caused by the slightly smaller effective force constant in the unperturbed KBr crystal. It is in excellent agreement with our experimental observation. The best fit to the measured frequencies is obtained with $A01 \gtrsim -0.50$ and $A14 \gtrsim +0.002$. The positive sign in the last value is at the limit of the accuracy of our calculation. However, we can see the tendency of $A14$ to increase when going from KI to KBr, while the change of the force constant to $1nn$ remains roughly the same. This supports our suggestions outlined above. $A01$ is primarily given by the formation of the vacancy. The additional contribution to $A01$ due to the outward or inward relaxation of $1nn$ is very small, whereas $A14$ is determined almost exclusively by the relaxation process. The small positive value $A14$ for KBr indicates that the relaxation of $1nn$ of the F center is much smaller than in KI, and may even be in the opposite direction. We will again consider this question briefly in Sec. VI.

Difficulties arise in the calculation of the intensities of the in-gap absorption. Because the derivatives of the Green's functions with respect to ω,

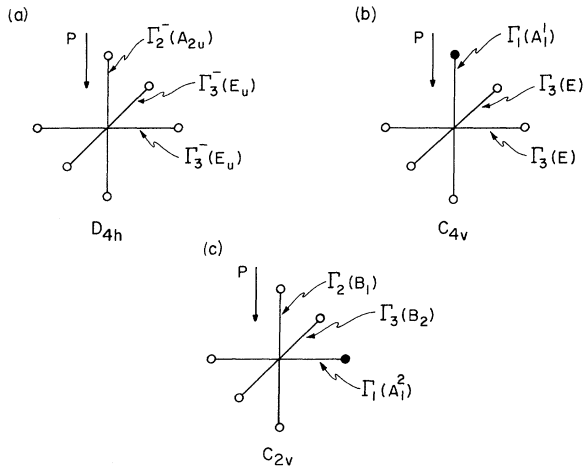

FIG. 6. Behavior of F centers in the $b(0)$ [case (a)] and $b(1)$ [cases (b) and (c)] configurations with uniaxial stress. ○ denotes K^{39} and ● denotes K^{41} isotopes. The single components of the split lines A and B contain

$P \parallel E$: $\nu_1^-(A) : \Gamma_2^-(A_{2u})$; $\Gamma_2(B_1)$
$\nu_1(B) : \Gamma_1(A_1')$ "shifted".

$P \perp E$: $\nu_2(A) : \Gamma_3^-(E_u)$; $\Gamma_3(E)$; $\Gamma_3(B_2)$
$\nu_2(B) : \Gamma_1(A_1^2)$; "slightly shifted".

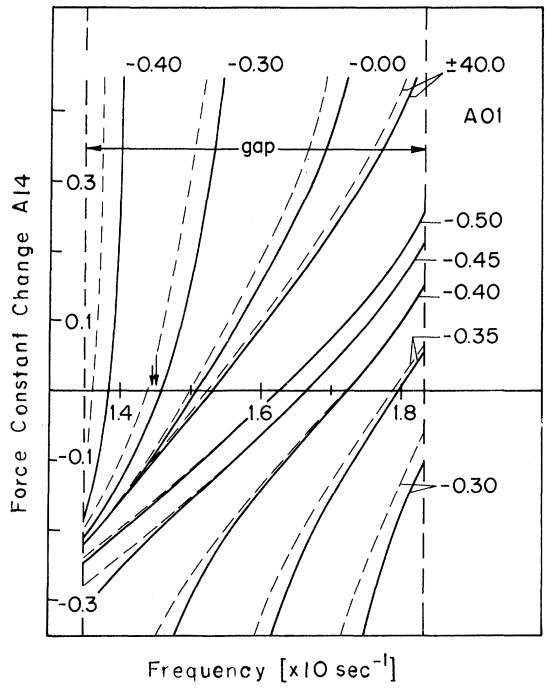

FIG. 7. Line position and isotope splitting for the gap modes due to Cl^{35} (solid line) and Cl^{37} (dashed line) centers in KI as a function of force-constant changes $A01$ and $A14$. The arrow shows the position of the doublet.

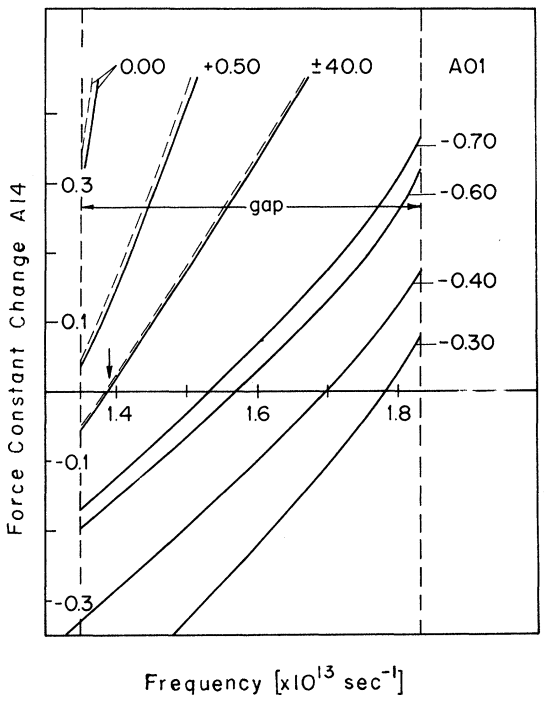

FIG. 8. Same as Fig. 6, but for Br^{79} and Br^{81} centers in KI.

which enter the equations, are much more inaccurate than the Green's functions themselves, this approach is not practical. However, an heuristic estimate of the relative intensities may be obtained in the following way: Denoting the probability that n F centers have i K^{41} ions as $1nn$ by $P_i(n)$, the average occupation number is then [21]

$$b(i)=\sum_n P_i(n)=k\binom{m}{i}(1-1/k)^{m-i}(1/k)^i .$$

For the natural abundance ratio of K^{39}: $K^{41}=93:7$, we obtain

$$b(0)=65.5\%;\quad b(1)=27.7\%;\quad b(2)=5.9\%.$$

In order to compare the relative frequencies of these three configurations with the relative intensities of the lines, one must take into account the polarization and the degree of degeneracy in the modes as indicated in Sec. IV, cases 2(a)–2(c). One then obtains

$$A=2b(0)+\tfrac{4}{3}b(1)+\tfrac{12}{15}b(2),$$

$$B=\tfrac{2}{3}b(1)+\tfrac{16}{15}b(2),$$

$$C=\tfrac{2}{15}b(2).$$

The above values then yield

$$I(A):I(B):I(C)=210:30:1.$$

This is in agreement with the experimental results of Sec. III A to within experimental error [compare Eqs. (3.1) and (3.2)].

B. Anharmonic Coupling Coefficients

From the slope of the function $\Delta\nu_{1,2}(A)=f(P)$ (see Sec. III B) for different directions of polarization we can determine two of the anharmonic coupling coefficients of the F-center-induced vibration to static distortions of the lattice.

Uniaxial stress in the [100] direction lowers the point symmetry for F centers in the $b(0)$ configuration from O_h to D_{4h}. In the $b(1)$ configuration the symmetry becomes C_{4v} for C axis $\parallel P$ and C_{2v} for C axis $\perp P$ (see Fig. 6). Centers in the $b(2)$ configuration shall be neglected in the following. But because no measurable splitting was observed between the Γ_2^- (A_{2u}) and $\Gamma_2(B_1)$ levels and among the $\Gamma_3^-(E_u)$, $\Gamma_3(E)$, and $\Gamma_3(B_2)$ levels, we will assume that the static distortions are nearly of $\Gamma_1^+(A_{1g})$, $\Gamma_3^+(E_g)$, and $\Gamma_5^+(T_{2g})$ symmetry. According to Ref. 22 we then obtain

$$\Delta\nu_1/\Delta P=\alpha(\bar{s}_{11}+2\bar{s}_{12})+4\beta(\bar{s}_{11}-\bar{s}_{12})$$

for $E\parallel P\parallel[100]$, and

$$\Delta\nu_2/\Delta P=\alpha(\bar{s}_{11}+2\bar{s}_{12})-2\beta(\bar{s}_{11}-\bar{s}_{12})$$

for $E\parallel[001]$, $P\parallel[100]$. α and β are the anharmonic

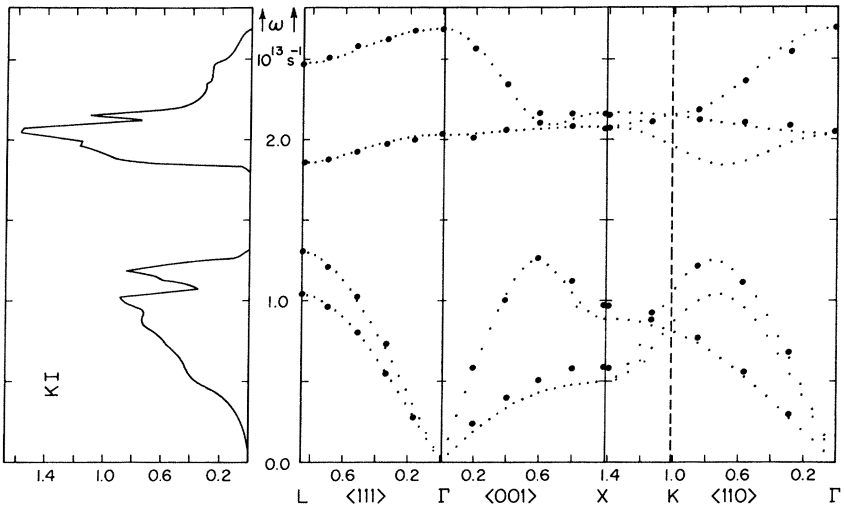

FIG. 9. Density of states and dispersion curves for KI as obtained with the Schröder model ($T = 0$ °K) denotes measured values according to Dolling *et al.* (Ref. 12).

coupling coefficients which transform like $\Gamma_1^+(A_{1g})$ and $\Gamma_3^+(E_g)$. $\bar{s}_{11}$, $\bar{s}_{12}$ are the local compliances. From Ref. 8 we obtain with $A01 = -0.57$, $A14 = -0.12$ the local stiffness constants

$$\bar{c}_{11} = 0.264 \times 10^{12} \text{ dyn/cm}^2; \quad \bar{c}_{12} = 0.032 \times 10^{12} \text{ dyn/cm}^2.$$

The local compliances are then

$$\bar{s}_{11} + 2\bar{s}_{12} = 3.05 \times 10^{-12} \text{ cm}^2/\text{dyn},$$

$$\bar{s}_{11} - \bar{s}_{12} = 5.00 \times 10^{-12} \text{ cm}^2/\text{dyn}.$$

Together with the measured values of $\Delta\nu_{1,2}(A)/\Delta P$, we obtain for the 82.62-cm^{-1} line

$$\alpha(\bar{s}_{11} + 2\bar{s}_{12}) = 0.037 \pm 0.01 \text{ cm}^{-1} \text{ mm}^2/\text{kg},$$

$$\beta(\bar{s}_{11} - \bar{s}_{12}) = 0.02 \pm 0.005 \text{ cm}^{-1} \text{ mm}^2/\text{kg},$$

or

$$\alpha = 125 \pm 40 \text{ cm}^{-1}; \quad \beta = 35 \pm 15 \text{ cm}^{-1}.$$

Therefore, the excited vibrational state of the F center is strongly coupled to spherical distortions. However, these values are only about one-eighth as large as the corresponding values for low-lying resonant modes, e. g., the Li mode in KBr.[23] Furthermore, we see that for the gap mode, where only anharmonic damping is possible, the half-width is determined by $\Gamma_1^+(A_{1g})$ distortions, which cause a small anharmonic frequency shift as well.

The shift in line B at 81.98 cm^{-1} depends on the relative orientation of P, E, and the c axis. The lifting of the configuration degeneracy with uniaxial stress can be seen from Fig. 6. For case (b) ($P \| c$ axis) the force constant A_{14} increases with applied stress. Therefore, we get a positive shift $\Delta\nu_1(B)$ of the $\Gamma_1(A_1^1)$ mode. This shift can be estimated by the well-known relation (see, e. g., Ref. 1)

$$-\frac{\partial \ln\omega}{\partial \ln a} = \frac{3\alpha}{\omega}$$

or

$$\delta\omega = 3A\,\delta a/a = 3\alpha P(\bar{s}_{11} + 2\bar{s}_{12}).$$

For 100 kg/cm^2, we get with the above values $\Delta\nu_1(B) \approx 0.1$ cm^{-1}, which is in good agreement with the measured value $\Delta\nu_1(B)$ in Sec. III B. For case (c) ($P \perp c$ axis) the orthogonal spring can increase or decrease. From the measured shift $\Delta\nu_2(B) \lesssim 0$, a small decrease in this force constant follows.

VI. COMPARISON WITH EARLIER RESULTS

In Ref. 8 Benedek and Mulazzi fit the force-constant pairs $A01$, $A14$ to the half-width of the electronic F band. They obtain $A01 = -0.57$, $A14 = -0.12$ for KI and $A01 = -0.43$, $A14 = -0.16$ for KBr. Comparing these force-constant pairs with the values obtained in Sec. V ($A01 = -0.50$, $A14 = -0.060$ for

TABLE I. F-center splitting in KI, $\omega_A = 1.556 \times 10^{13}$ sec^{-1}.

$A01$	$A14$	ω_B	ω_C	Δ_{AB}	Δ_{AC}
− 0.60	+0.070	1.545	1.540	0.011	0.016
− 0.50	−0.060	1.545	1.528	0.011	0.028
− 0.40	−0.103	1.547	1.532	0.009	0.024
− 0.33	−0.132	1.546	1.520	0.010	0.036
0.00	−0.165	1.542	1.520	0.014	0.036
± 40.0	−0.205	1.545	1.525	0.011	0.031
− 1.00	−0.292	1.555	1.535	0.001	0.021
− 0.80	−0.412	1.605	1.590	−0.049	−0.034

TABLE II. F-center splitting in KBr, $\omega_A = 1.8761 \times 10^{13}$ sec^{-1}.

$A01$	$A14$	ω_B	ω_C	Δ_{AB}	Δ_{AC}
− 0.70	+0.170	1.868	1.862	0.008	0.014
− 0.50	+0.002	1.864	1.856	0.012	0.020
− 0.30	−0.058	1.866	1.856	0.010	0.020
0.00	−0.104	1.866	1.856	0.010	0.020
+ 2.00	−0.164	1.866	1.856	0.010	0.020
±40.0	−0.198	1.866	1.856	0.010	0.020

KI and $A01 = -0.50$, $A14 = +0.002$ for KBr) we get an agreement in the $A01$ values within ± 15%. However, a large difference in the $A14$ values is revealed. For KBr, $A14$ even tends to be of opposite sign. This disagreement is probably due to the insensitivity of the half-width of the electronic band to changes in $A14$. On the other hand, if we fit the calculations outlined in Ref. 8 to the measured in-gap–mode frequencies – keeping $A01$ constant – we obtain $A14 = -0.13$ for KI and $A14 = +0.04$ for KBr.

In order to estimate the relaxation of $1nn$ around the F center we follow our argumentation in Sec. V. In a first approximation the relaxation is given by the repulsive part of the ionic interaction potential which varies according to Born-Mayer as $e^{-r/\rho}$. For the change in the distance between $1nn$ and $4nn$ we then obtain

$$\delta r_{14} = -(\rho/A)\,\delta\varphi''_{14} ,$$

with $\delta\varphi''_{14} = (A14)\times A$; $\rho(\mathrm{KI}) = 0.349$ Å; and $\rho(\mathrm{KBr}) = 0.334$ Å. This means that within this assumption an inward relaxation of $1nn$ in KI of 0.6–1.2% and an outward relaxation of $1nn$ in KBr of 0.02–0.4% is most likely. The outward relaxation of $1nn$ in KBr is supported by elastic calculations by Thommen[24] (+0.6%) and by volume-expansion measurements by Lüty *et al.*[25] who use the Eshelby model[26] for explaining the relative volume increase when U centers are converted to F centers in KBr (+3.2%). The "large" value reported in Ref. 25 may be due in part to the interstitial H_2 molecules – created in the U-F conversion – producing a further increase in the lattice. Moreover, the volume-expansion measurements were carried out at a much higher temperature, 77 and 300 °K, respectively, than our measurements and calculations which were done at 1.2 and 0 °K, respectively. For KI, no analogous calculations or measurements are known.

To further test the model calculations of Sec. IV, we calculate the isotope splitting of the in-gap modes due to Cl^{35} and Cl^{37} centers and Br^{79} and Br^{81} centers in KI.

Figures 7 and 8 show the results of these calculations. The splitting into two bands observed for Cl^- can be described correctly only by taking $4nn$ force-constant changes into account. With $A14 = 0$ the observed position is found with $A01 = -0.31$; however, the calculated splitting is then too large by a factor of about 4 to 5 with respect to the experimental values. But additionally the observed splitting can also be found when a change in $A14$ is allowed. An interesting feature occurs in the Cl^- calculation in the range of $-0.25 < A14 < +0.15$. Two solutions are found simultaneously: one mode splits from the acoustic band, whereas the other one splits from the optical band.

The isotope splitting of Br^- centers becomes much smaller. Over nearly the whole range of parameters used in the calculation the splitting was less than $0.002\times10^{13}\,\mathrm{sec}^{-1} \triangleq 0.1\,\mathrm{cm}^{-1}$. This result is in good agreement with the upper limit of the splitting as estimated by Nolt *et al.*[13] At this time, the force-constant parameters in these cases can be fixed only by comparing calculated and measured in-band resonances. This is due to the limited accuracy of the calculation as was previously mentioned for KBr with F centers, and is especially true for the small isotope splitting for Br^- centers in KI. A second source of uncertainty is the limited resolution of the measurements.

ACKNOWLEDGMENTS

The authors wish to thank Professor H. Haken and Professor H. Pick for their support of this work. We are indebted to Professor M. Wagner and D. Kühner for helpful discussions, and to Dr. D. Strauch for placing the breathing-shell-model program at our disposal. For one of us (D. B.) it is a pleasure to also acknowledge valuable discussions with Professor A. J. Sievers, Professor R. O. Pohl, and Dr. E. Mulazzi. We wish to thank R. Blewitt for reading the manuscript.

APPENDIX

We describe the lattice dynamics of the unperturbed crystal by the breathing-shell model introduced by Schröder.[11] The eigenvectors and frequencies are calculated at 64 000 points in the Brillouin zone. We took the following parameters for the calculation: For KI: $m_K = 39.102$, $m_I = 126.9044$ (relative ion masses),

$a_0 = 3.489\times10^{-8}$ cm (distance between nearest neighbors),

$c_{11} = 0.338\times10^{12}$ dyn/cm^2 (elastic constants),

$c_{12} = 0.022\times10^{12}$ dyn/cm^2,

$c_{14} = 0.0368\times10^{12}$ dyn/cm^2,

$\alpha_1 = 1.201\times10^{-24}$ cm^3, $\alpha_2 = 6.199\times10^{-24}$ cm^3 (the polarizability of the K^+ and I^- ion, respectively,)

$ZZ = 0.90$ (relative ionic charge),

$\omega_{TO} = 2.035\times10^{13}\,\mathrm{sec}^{-1}$ (infrared eigenfrequency),

$\epsilon_0 = 4.74$, $\epsilon_\infty = 2.71$ (the static and high-frequency dielectric constants, respectively).

The effective force constants were $A = 13.8718\,e^2/2v_0$ and $B = -1.0389e^2/2v_0$.

Figure 9 shows the density of states together with the dispersion curves along major symmetry directions in KI at $T = 0$ °K. The ordinate for the density is in arbitrary units with the condition that the area under the curve is normalized to unity. The shape of the single branches of the dispersion

curves is compared with neutron scattering data as reported in Ref. 12. The splitting in TO and TA branches in the [110] direction was not measured.

*Work supported by the U. S. Atomic Energy Commission under Contract No. AT (30-1)-2391, Technical Report No. NYO-2391-115. Additional support was received from the Advanced Research Projects Agency through the Materials Science Center at Cornell University, Report No. 1331.

†Work done in part at the II. Physikalisches Institut der Universität Stuttgart, Germany.

‡"Max Kade Research Fellow" of the Max Kade Foundation of New York.

§Present address: Interatom, 506 Bensberg/Köln, Germany.

[1]A. J. Sievers, in *Proceedings of the International Conference on Localized Excitations in Solids* (Plenum, New York, 1968).

[2]E. J. Woll, T. Gethins, and T. Timusk, Can. J. Phys. 46, 2263 (1968).

[3]D. Bäuerle and B. Fritz, Solid State Commun. 6, 453 (1968); Phys. Status Solidi 29, 639 (1968).

[4]U. Dürr and D. Bäuerle, Z. Physik 233, 94 (1970).

[5]M. V. Klein, in *Color Centers in Alkali Halides*, edited by W. B. Fowler (Academic, New York, 1968).

[6]J. B. Page and D. Strauch, Phys. Status Solidi 24, 469 (1967).

[7]G. Benedek and G. F. Nardelli, Phys. Rev. 155, 1004 (1967).

[8]G. Benedek and E. Mulazzi, Phys. Rev. 179, 906 (1969).

[9]R. Hübner, Z. Physik 222, 380 (1969).

[10]C. H. Henry, S. E. Schnatterly, and C. P. Slichter, Phys. Rev. 137, 568 (1965).

[11]U. Schröder, Solid State Commun. 4, 347 (1966).

[12]G. Dolling, R. A. Cowley, C. Schittenhelm, and I. M. Thorson, Phys. Rev. 147, 577 (1966).

[13]I. G. Nolt, R. A. Westwig, R. W. Alexander, and A. J. Sievers, Phys. Rev. 157, 730 (1967).

[14]K. Johnson, R. Weber, and A. J. Sievers (unpublished).

[15]L. Genzel (unpublished).

[16]D. Kühner and M. Wagner, Z. Physik 207, 111 (1968).

[17]A rough picture for a shell consists of all lattice ions which have the same distance from the center. However, sometimes there exist ions with the same distance which do not belong to the same shell (see, e.g., Ref. 9).

[18]This model is only true as long as the changes in the force constants and effective charges can be considered as independent parameters.

[19]R. A. Cowley and W. Cochran, Phys. Rev. 131, 1030 (1963).

[20]A. A. Maradudin, E. W. Montrol, and G. H. Weiss, *Solid State Physics* (Academic, New York, 1963).

[21]R. V. Mises, Vorlesungen 1, (1931).

[22]W. Gebhardt and K. Maier, Phys. Status Solidi 8, 303 (1965).

[23]I. G. Nolt and A. J. Sievers, Phys. Rev. Letters 16, 1103 (1966).

[24]K. Thommen, Z. Physik 186, 347 (1965).

[25]F. Lüty, S. Mascarenhas, and C. Ribeiro, Phys. Rev. 168, 1080 (1968).

[26]J. Eshelby, Solid State Phys. 3, 79 (1956).

PHYSICAL REVIEW B VOLUME 2, NUMBER 10 15 NOVEMBER 1970

Theory for the Interaction of Phonons with Nonharmonic Impurities and Their Effect on the Polarizability

Manuel Gomez-Rodriguez*
Naval Research Laboratory, Washington, D.C. 20390

(Received 23 October 1969)

A new formalism is used to describe the interaction of localized nonharmonic impurities with a field. The impurity is described in terms of anticommuting Fermi operators, thus permitting the use of diagrammatic techniques. The formalism is used to study the impurity-phonon interaction in general, and to study, in particular, the effect of the phonon field on the impurity's polarizability. Using linear-response theory and thermodynamic Green's functions, the polarizability is obtained. It is found to contain a resonance term and a dipole relaxation term which is found to be present even when the impurity has no diagonal dipole matrix elements. The effect of the four-vertex part on the polarizability is to renormalize the impurity's dipole matrix elements and make them temperature dependent. The formalism is particularly suited to the study of highly polarizable impurities such as the proton in hydrogen-bonded ferroelectrics, off-center impurities, and permanent-dipole impurities.

I. INTRODUCTION

The interaction of the phonon field with a localized nonharmonic impurity having a finite number of physically relevant quantum-mechanical (QM) levels and the interaction of these two systems with the electromagnetic field form an important class of problems occurring in solid-state physics. It will prove particularly useful to calculate physical properties such as the polarizability of the impu-